

Design, optimization and simulation of a low-voltage shunt capacitive RF-MEMS switch

Li-Ya Ma¹ · Anis Nurashikin Nordin² · Norhayati Soin¹

Received: 29 June 2014 / Accepted: 29 May 2015 / Published online: 16 June 2015
© Springer-Verlag Berlin Heidelberg 2015

Abstract This paper presents the design, optimization and simulation of a radio frequency (RF) micro-electro-mechanical system (MEMS) switch. The capacitive RF-MEMS switch is electrostatically actuated. The structure contains a coplanar waveguide, a big suspended membrane, four folded beams to support the membrane and four straight beams to provide the bias voltage. The switch is designed in standard 0.35 μm complementary metal oxide semiconductor process and has a very low pull-in voltage of 3.04 V. Taguchi method and weighted principal component analysis is employed to optimize the geometric parameters of the beams, in order to obtain a low spring constant, low pull-in voltage, and a robust design. The optimized parameters were obtained as $w = 2.5 \mu\text{m}$, $L1 = 30 \mu\text{m}$, $L2 = 30 \mu\text{m}$ and $L3 = 65 \mu\text{m}$. The mechanical and electrical behaviours of the RF-MEMS switch were simulated by the finite element modeling in software of COMSOL Multiphysics 4.3[®] and IntelliSuite v8.7[®]. RF performance of the switch was obtained by simulation results, which are insertion loss of -5.65 dB and isolation of -24.38 dB at 40 GHz.

1 Introduction

Radio-frequency (RF) micro-electro-mechanical system (MEMS) switches operating at RF to millimetre-wave frequencies have many advantages over p-i-n diode or field-effect transistor (FET) switches, such as low or near-zero power consumption, high isolation, low insertion loss, and high linearity (Lee et al. 2006). These RF-MEMS switches use mechanical movements to short or open a transmission line; and normally can be integrated with a planar or coplanar waveguide (CPW).

There are many varieties of RF-MEMS switches. The switch can be in series or in shunt connected with the signal path; coupling method can be either capacitive or metal-to-metal (Chan et al. 2003); and actuation mechanism can be electrostatic (Kim et al. 2010), electromagnetic (Glickman et al. 2011), thermal (Daneshmand et al. 2009), piezoelectric (Park et al. 2006) or combined actuations (Cho and Yoon 2010). Electrostatic actuated RF-MEMS switches are the most prevalent technique in use today; due to their virtually zero power consumption, high switching speed (Kim et al. 2010), small electrode size, thin layers used, 50–200 μN of achievable contact forces, the possibility of biasing the switch using high-resistance bias lines (Rebeiz 2003), and the high compatibility with a standard Integrated Circuitry (IC) process (Chu et al. 2007). However, the largest challenge for electrostatic switches is their relative high actuation (or pull-in) voltage, which is around 20–80 V (Lee et al. 2006; Kim et al. 2010; Park et al. 2006; Mafinejad et al. 2013).

Usage of standard complementary metal-oxide semiconductor (CMOS) technologies have always been of great interest for the implementation of RF-MEMS devices due to their mature fabrication process, higher levels of integration, and also lower manufacturing cost (Fouladi and

✉ Li-Ya Ma
maliya8445@gmail.com

Anis Nurashikin Nordin
anisnn@iium.edu.my

Norhayati Soin
norhayatisoin@um.edu.my

¹ Department of Electrical Engineering, University of Malaya, 50603 Kuala Lumpur, Malaysia

² Department of Electrical and Computer Engineering, International Islamic University Malaysia, 53100 Kuala Lumpur, Malaysia

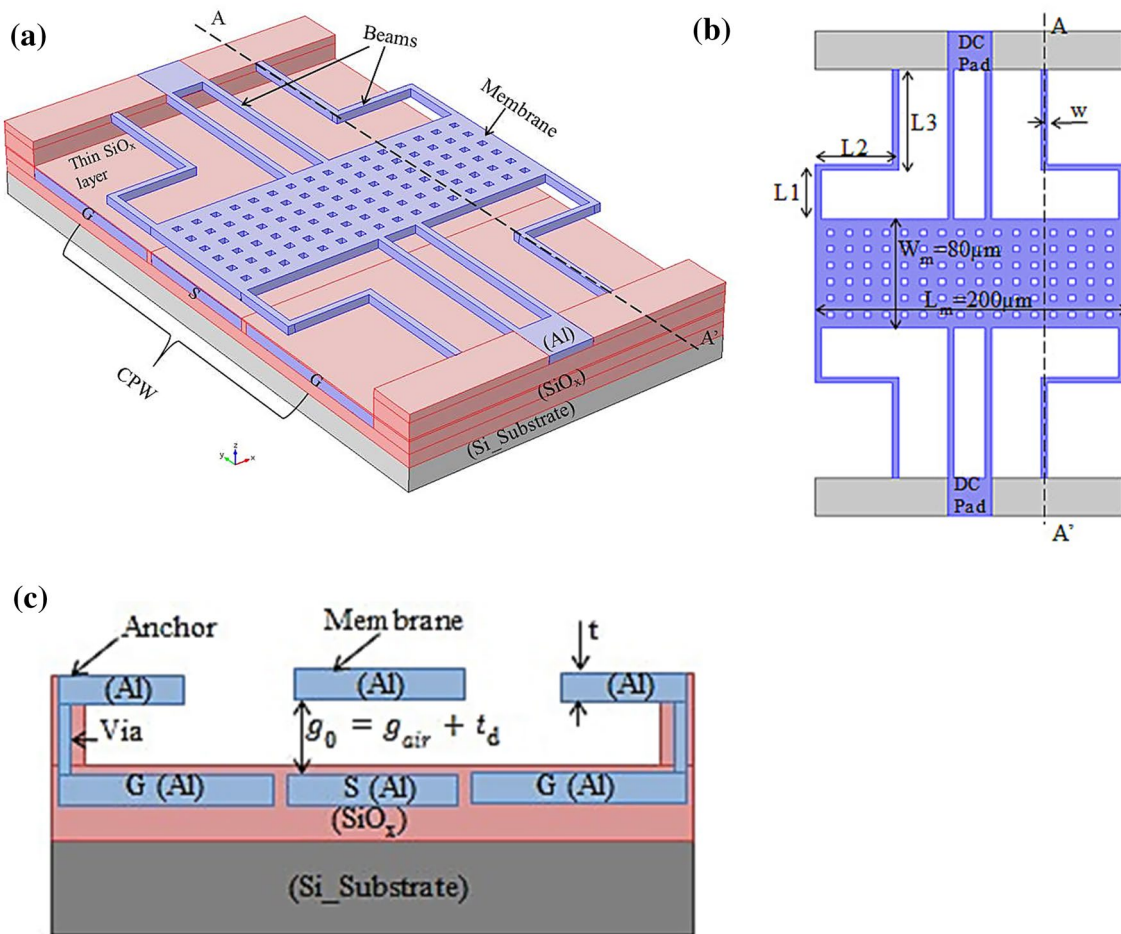


Fig. 1 RF-MEMS switch design. **a** Overall view, **b** top view and **c** cross-section view (A–A')

Table 1 Each layer thickness

Name	Membrane (t)	Dielectric layer (td)	CPW lines	Air gap (g)
Thickness	0.877 µm	0.1 µm	0.624 µm	1.397 µm

Table 2 Geometric parameters with their possible values

Factor	Level 1 (µm)	Level 2 (µm)	Level 3 (µm)
Beam width (w)	2	2.5	3
First length (L1)	20	25	30
Second length (L2)	30	35	40
Third length (L3)	60	65	70

Mansour 2010). Nevertheless, generally standard 0.35 µm CMOS process fabricated devices require compatible operating voltage supply of 3.3 V or less than 3.3 V (Yusoff et al. 2004; Wey et al. 2002), which is insufficient to actuate the most developed electrostatically-actuated RF-MEMS

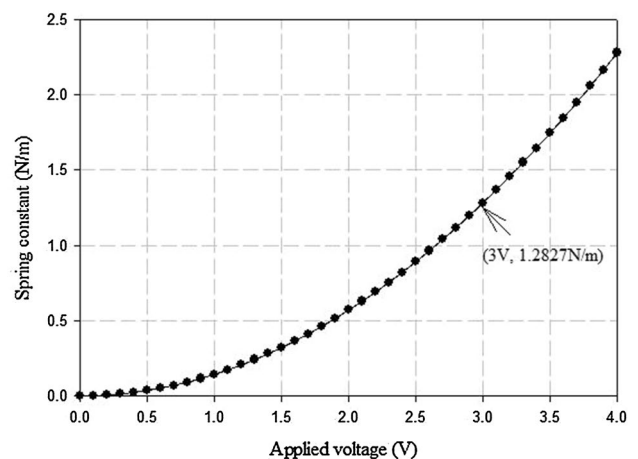


Fig. 2 Relationship of V_p and k

switches. In order to monolithically integrate these RF-MEMS switches with active CMOS circuitry, an additional voltage-upconverter or an external off-chip circuit is needed

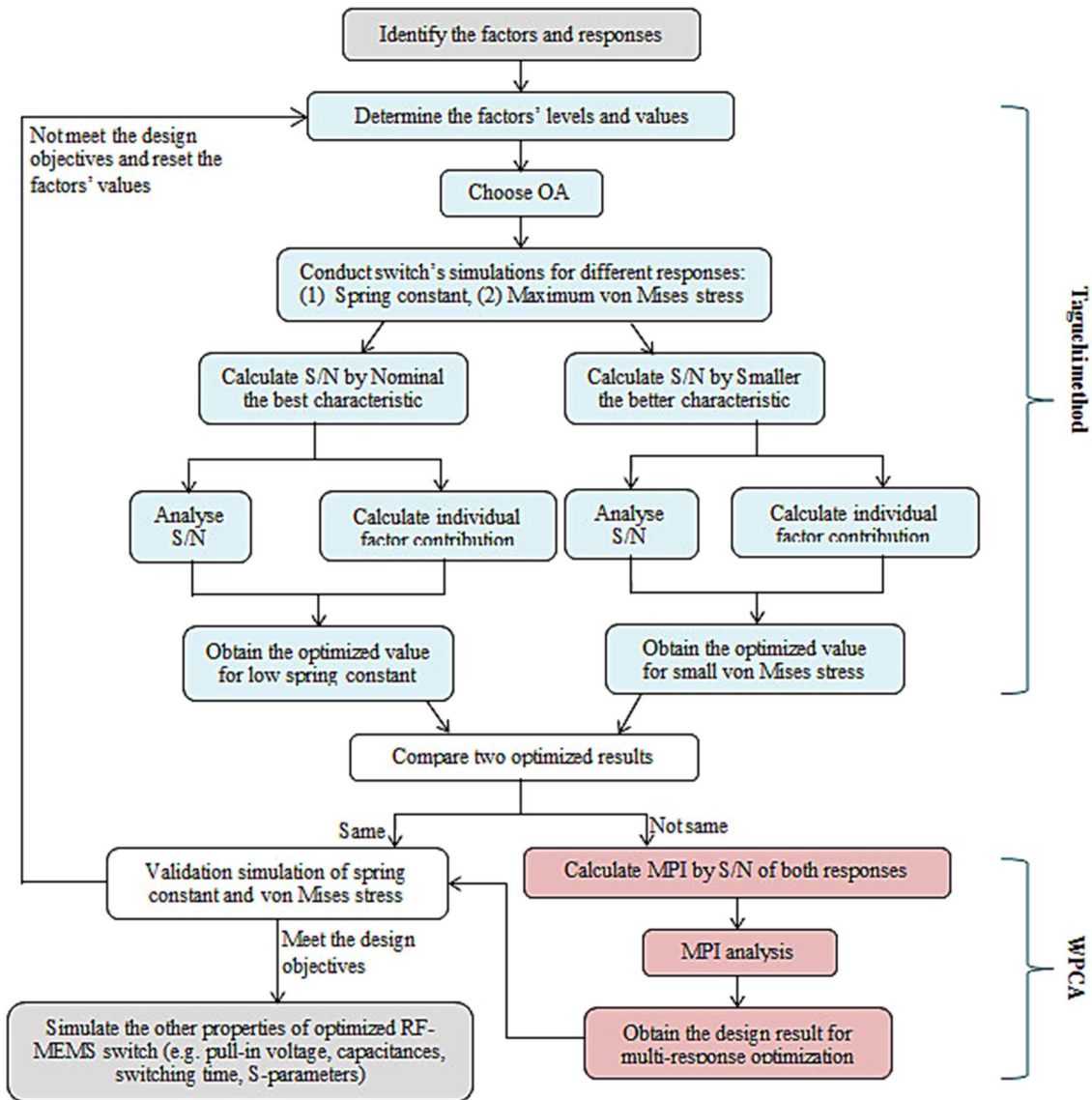


Fig. 3 Multi-response optimization methodology

Table 3 Simulated results of spring constant (k) and maximum von Mises stress ($\sigma_{v(max)}$) with their corresponding S/N

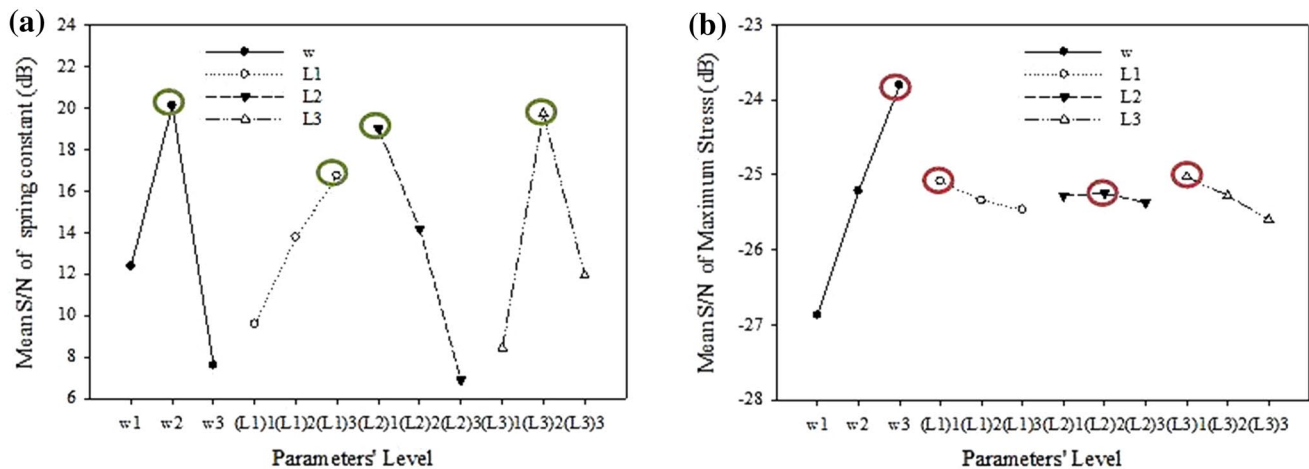
Simulation no.	Parameter				Simulation results		Calculated S/N	
	w	L1	L2	L3	k (N/m)	$\sigma_{v(max)}$ (MPa)	k (dB)	$\sigma_{v(max)}$ (dB)
1	1	1	1	1	1.625	20.800	9.302	-26.361
2	1	2	2	2	1.182	21.987	19.939	-26.843
3	1	3	3	3	0.877	23.477	7.840	-27.413
4	2	1	2	3	1.446	18.306	15.740	-25.252
5	2	2	3	1	1.633	17.900	9.121	-25.057
6	2	3	1	2	1.300	18.496	35.494	-25.342
7	3	1	3	2	1.935	15.219	3.707	-23.648
8	3	2	1	3	1.528	16.081	12.220	-24.126
9	3	3	2	1	1.737	15.217	6.861	-23.647

$\sigma_{v(max)}$ is obtained with 1 μ N surface load

Table 4 Average values of S/N ratio for each response

Parameter	Mean S/N ratio for k (dB)				Parameter	Mean S/N ratio for $\sigma_{v(max)}$ (dB)			
	Level 1	Level 2	Level 3	Max-Min		Level 1	Level 2	Level 3	Max-Min
w	12.360	20.118	7.596	12.522	w	-26.873	-25.217	-23.807	3.066
L1	9.583	13.760	16.732	7.149	L1	-25.087	-25.342	-25.467	0.380
L2	19.005	14.180	6.890	12.116	L2	-25.276	-25.247	-25.373	0.125
L3	8.428	19.713	11.934	11.286	L3	-25.022	-25.278	-25.597	0.575

For each parameter, the bold values are the largest mean S/N ratio among three levels, as highlighted corresponding point in Figs. 4 and 6

**Fig. 4** Mean S/N plots. **a** Mean S/N of spring constant and **b** Mean S/N of maximum von Mises stress

(Lee et al. 2006), which will make the whole chip larger, more complex, and consume more power. Chan et al. and Goldsmith et al. indicated that a high actuation voltage also may lead to a shorter lifetime for capacitive RF-MEMS switches which use dielectric layers for isolation (Shalaby et al. 2009). Diverse RF-MEMS switch designs have been proposed by various researchers to reduce the actuation voltages. A dedicated RF-MEMS switch fabricated in 0.35 μm CMOS process has been reported to require a pull-in voltage of 7 V (Dai and Chen 2006). A bi-stable RF-MEMS switch was designed with a low actuation voltage of 5 V, but was not compatible with CMOS process (Lakamraju and Phillips 2005). Afrang et al. (Afrang and Abbaspour-Sani 2006) have introduced a CMOS fabricated membrane-based switch with actuation voltage of 12.5 V. Authors' previous design on CMOS RF-MEMS switch managed to achieve a low pull-in voltage of 3 V (Ya et al. 2013), however, the relatively wide beams cannot be easily released with membrane in one step; an additional mask wet etch is needed. Moreover the long membrane design is hard to keep it in-plane during fabrication and operation which deteriorates a lot in its RF performance.

In this paper, an advanced low-voltage electrostatically-actuated shunt capacitive RF-MEMS switch is proposed by using MIMOS (Malaysia Institute of Microelectronic

Systems) standard 0.35 μm (double poly triple metal) CMOS technology. The actuation voltage of 3.04 V was achieved by reduction of the beams' spring constant while maintaining the structure's robust using multi-response optimization method, which comprises Taguchi method and weighted principal component analysis (WPCA). The rest of the paper is divided into the following sections: Sect. 2 presents the detail designs of RF-MEMS switch. Section 3 displays the beams' geometric optimization by Taguchi method and WPCA. Section 4 illustrates the simulation results of applied voltage with the membrane displacement, stress distributions, switching time, switch-on and switch-off capacitances, insertion loss and isolation, as well as a comparison of the designed switch with other related work.

2 RF-MEMS switch design

The structure of the RF-MEMS switch is illustrated in Fig. 1a. The RF-MEMS switch consists of a membrane, four folded beams, four straight beams, anchors and coplanar waveguide (CPW) lines. The four folded beams mainly provide support to the large membrane and the four straight beams are used to supply the DC bias. Figure 1b displays the geometric parameters of the membrane and beams,

Fig. 5 Percentage contribution of each factor to the both responses. **a** Spring constant, and **b** Maximum von Mises stress

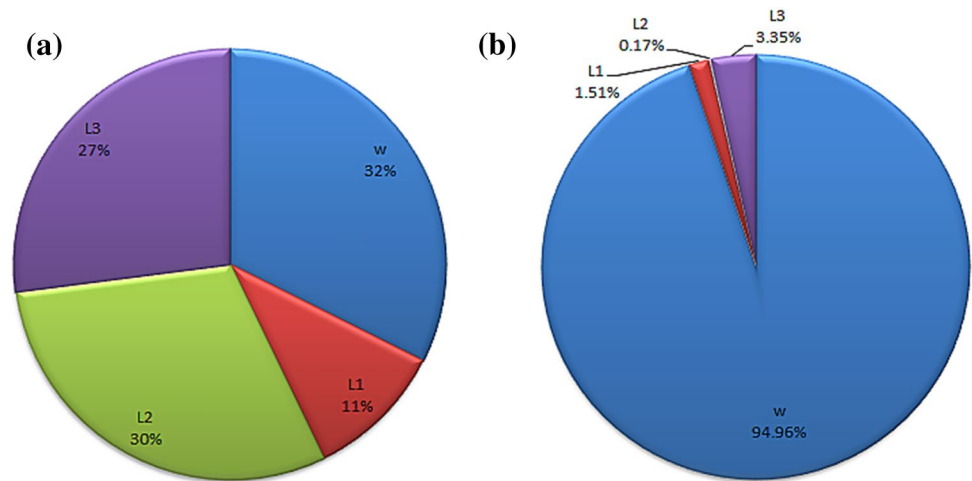


Table 5 Normalized S/N values and computed MPI

Simulation No	Parameter				Normalized S/N		MPI
	w	L1	L2	L3	$k(x_i^*(1))$	$\sigma_{v(max)}(x_i^*(2))$	
1	1	1	1	1	0.1760	0.2792	0.0774
2	1	2	2	2	0.5107	0.1512	0.3356
3	1	3	3	3	0.1300	0.0000	0.0919
4	2	1	2	3	0.3786	0.5738	0.1710
5	2	2	3	1	0.1703	0.6255	0.0151
6	2	3	1	2	1.0000	0.5500	0.6145
7	3	1	3	2	0.0000	0.9997	-0.1684
8	3	2	1	3	0.2678	0.8726	0.0424
9	3	3	2	1	0.0992	1.0000	-0.0983

Table 6 Explained variation and eigenvector

Principal component	Eigen value	Explained variation (%)	Cumulative variation (%)	Eigenvector [k, $\sigma_{v(max)}$]
Z1	1.238	61.913	61.913	[0.707, -0.707]
Z2	0.762	38.087	100.000	[0.707, 0.707]

where the holes are used to release the membrane during the post-CMOS process. And Fig. 1c shows the cross-section view of the switch, where the four folded beams are connected to the ground lines of the CPW by via; and a very thin dielectric layer covers the CPW lines to consist the coupling capacitor during actuated state.

When a DC bias voltage is applied between the membrane and signal line, there is a positive feedback between the electrostatic forces and the deformation of the membrane. The applied voltage creates electrostatic forces that bend down the beam and thereby reducing the gap to the ground substrate. The reduced gap between the membrane and signal line, in turn, increases the electrostatic forces. At a certain voltage, the electrostatic force overcomes the mechanical stress limit of the beam causing the system to

be unstable, and the gap collapses. This critical voltage is called pull-in voltage or actuation voltage (V_p) and can be described as shown in (1) (Rebeiz 2003; Gupta 1997). Once the switch is actuated, a coupling capacitor induced between the membrane and signal line prevents the signal to be passed the signal line.

$$V_p = \sqrt{\frac{8kg_0^3}{27\epsilon_0A}} \tag{1}$$

where, k is the spring constant of the membrane and beams; g_0 is the initial gap between the membrane and the signal line; ϵ_0 is the permittivity of air, 8.854×10^{-12} F/m; and A is the area of the membrane, namely the product of the membrane’s width and length ($W_m \times L_m$).

Table 7 Average MPI for each factor at each level

Factor	MPI			Max-Min
	Level 1	Level 2	Level 3	
w	0.168	0.267	-0.075	0.342
L1	0.027	0.131	0.203	0.176
L2	0.245	0.136	-0.020	0.265
L3	-0.002	0.261	0.102	0.262

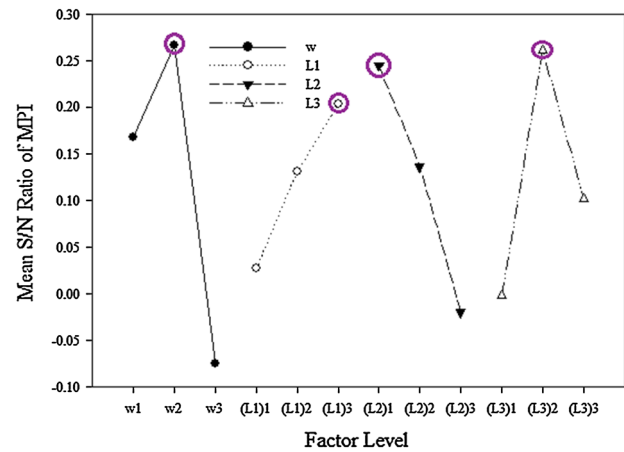
For each parameter, the bold values are the largest mean S/N ratio among three levels, as highlighted corresponding point in Figs. 4 and 6

The materials and thickness of each layer are determined by the CMOS fabrication process and is listed in Table 1. The membrane and CPW lines are made from aluminum (Al) and built by Metal3 and Metal1 layers of the standard process. The permittivity of the dielectric material between two metal layers is 4.99.

From (1) it can be seen that to achieve a low V_p , the capacitive switch should have a small spring constant (k), large membrane area (A) and big initial gap (g_0). In this design, the initial gap is determined by the CMOS process ($g_0 = g_{air} + t_d$); the membrane area is generally decided by the coupling capacitance which is in pF range and does not have much space and flexibility to be modified here. Therefore, the main parameter that can be designed and controlled by the researchers is the spring constant (Dai and Chen 2006; Peroulis et al. 2003; Balaraman et al. 2002; Kuwabara et al. 2006; Jaafar et al. 2009). The relationship of V_p and k can be observed in Fig. 2. Basically, in order to own a lower spring constant, the beam should have a less beam width or thinner beam thickness; but this will make the structure to become fragile and short-lived (Bao 2000). Optimization of beam lengths $L1$, $L2$ and $L3$, as well as beam width w to obtain a low spring constant while maintain a robust structure becomes an important problem for this low V_p RF-MEMS switch design.

3 Multi-response optimization method

There are four geometric parameters in the RF-MEMS switch as shown in Fig. 1b and the possible dimensions are listed in Table 2. These parameters need to be modified to obtain a low k and small maximum von Mises stress ($\sigma_{v(max)}$) simultaneously, where the low k can led to a low V_p as shown in Fig. 2 and the small $\sigma_{v(max)}$ can guarantee a robust structure (Chen and Harichandran 1998). Since every geometric parameter could be set with three different values, it will be tedious to simulate all their possible combinations ($3^4 = 91$ times). Therefore, a proper optimization technique is necessary here; it is also a general problem to be encountered by most RF-MEMS switches' design

**Fig. 6** Mean value of MPI

(Shalaby et al. 2009; Philippine et al. 2013). The only difference from each work could be the optimized responses (such as switching speed, power handling capability or RF performance) (Shalaby et al. 2009; Badia et al. 2012) or geometric design (shapes or dimensions) (Peroulis et al. 2003; Gong et al. 2009).

In this work, a multi-response optimization method which comprises Taguchi method and WPCA was employed to optimize the responses of the spring constant and maximum von Mises stress. This method could be simply implemented into other optimization problems which have single or multiple responses with diverse parameters. Figure 3 shows the multi-response optimization methodology. The optimized values are based on a 3-D structural-Electro-mechanics Finite Element Modeling (FEM) simulation results.

3.1 Taguchi method

Taguchi's parameter optimization is an important method for robust design. Taguchi defines robustness as the "insensitivity of the system performance to parameters that are uncontrollable by the designer" (Taguchi et al. 1987). A robust design incorporates this concept of robustness into design optimization and aims at achieving designs that optimize given performance measures while minimizing sensitivities against uncontrollable parameters using different approaches, such as signal to noise ratio (Shalaby et al. 2009). The Taguchi approach itself can be utilized to determine the best parameters for the optimum design configuration with the least number of analytical investigations. Comparing with other optimization methods, such as Genetic Algorithm (GA) (Li et al. 2003) or Neural Network (Meng and Butler 1997), the proposed multi-response optimization does not need much statistical or technical background in that specific

Table 8 Geometric parameters’ setting with different motivated optimization

Factor	The lowest spring constant design (model a) (μm)	The smallest von Mises stress design (model b) (μm)	The multi-response optimization design by WPCA (model c) (μm)
w	2.5	3	2.5
L1	30	20	30
L2	30	35	30
L3	65	60	65

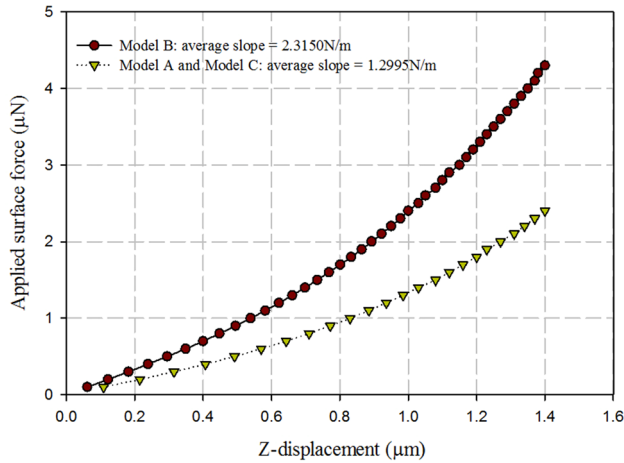


Fig. 7 Spring constant simulations for the optimized models

field, which can be easily implemented by engineering researchers (Roy 2010; Liao 2006). This method has not been widely employed for the optimization of RF-MEMS switch geometry but is more commonly used for process or product optimization. There are two major tools to be used in this method, which are orthogonal array (OA) and signal-to-noise ratio (S/N).

The folded and straight beams of the RF-MEMS switch will be analysed in terms of whole system’s k and $\sigma_{v(max)}$. In order to develop a RF-MEMS switch which could be implemented together with normal active CMOS circuitry as mentioned in part 1, a V_p of 3 V is proposed. From Fig. 2, it can be seen that for our model, a $V_p = 3$ V RF-MEMS switch should have a k of 1.2827 N/m. Therefore, in Taguchi method, the S/N of k is calculated according to the characteristics of the nominal the best; such a ratio is selected when a specific target value is desired. The optimum of $\sigma_{v(max)}$ on the other hand employed the smaller the better characteristic. This is because in order to avoid the structure failure, with the applied voltage load, the beams and membrane’s total $\sigma_{v(max)}$ should be less than their material’s yield strength (Chen and Harichandran 1998). With smaller $\sigma_{v(max)}$, the structure experiences less stretch. The

equations of both characteristics are shown in (2) and (3), respectively (Roy 2010).

Nominal the best:

$$S/N = -10 \log_{10} \left[\frac{(y_1 - y_0)^2 + (y_2 - y_0)^2 + \dots + (y_n - y_0)^2}{n} \right] \quad (2)$$

Smaller the better:

$$S/N = -10 \log_{10} \left[\frac{y_1^2 + y_2^2 + \dots + y_n^2}{n} \right] \quad (3)$$

where y_1, y_2, \dots are the simulation results, $y_0 = 1.2827$ N/m is the target value of results; and n is the number of observations with the same values of factors (here $n = 1$).

According to OA selector (Fralely et al. 2006), with four parameters and three levels of each parameter, OA of L_9 is selected as shown in Table 3, where the level of “1”, “2” and “3” under parameter columns represent the corresponding parameter’s least, middle and largest values. The OA of Taguchi method has the capability to reduce the full factorial designs into highly fractionated factorial designs and to make the design of experiments very easy and consistent. In Table 3, each row signifies random single simulation run that has been carried out. The simulation results for both responses of spring constant and maximum von Mises stress were obtained by FEM simulations using software of Comsol Multiphysics 4.3®, where Electro-mechanics model was employed with the boundary condition of eight beams’ end fixed. By applying (2) and (3) for simulated k and $\sigma_{v(max)}$, the S/N for each simulation run can be calculated as listed in Calculated S/N columns. In order to get the parameters’ optimum condition for each response, the average S/N at each level for k and $\sigma_{v(max)}$ are calculated separately in Table 4 and plotted in Fig. 4. For all of these characteristics, the largest value of S/N represents a more desirable condition (Roy 2010); and the bigger Max–Min value means that corresponding parameter has more effect on the response, vice versa.

Figure 4a suggests that in order to obtain the desired spring constant of 1.2827 N/m, the four parameters should be set as: $w = w_2 = 2.5 \mu\text{m}$, $L1 = (L1)_3 = 30 \mu\text{m}$, $L2 = (L2)_1 = 30 \mu\text{m}$ and $L3 = (L3)_2 = 65 \mu\text{m}$. Figure 4b illustrates that to obtain a structure with smallest von Mises stress and longer lifetime, the parameters should be set as: $w = w_3 = 3 \mu\text{m}$, $L1 = (L1)_1 = 20 \mu\text{m}$, $L2 = (L2)_2 = 35 \mu\text{m}$ and $L3 = (L3)_1 = 60 \mu\text{m}$. The contribution of each parameter to the spring constant and von Mises stress was calculated using Pareto analysis of variance (ANOVA) technique (Park and Antony 2008) and is shown in Fig. 5. These optimization results

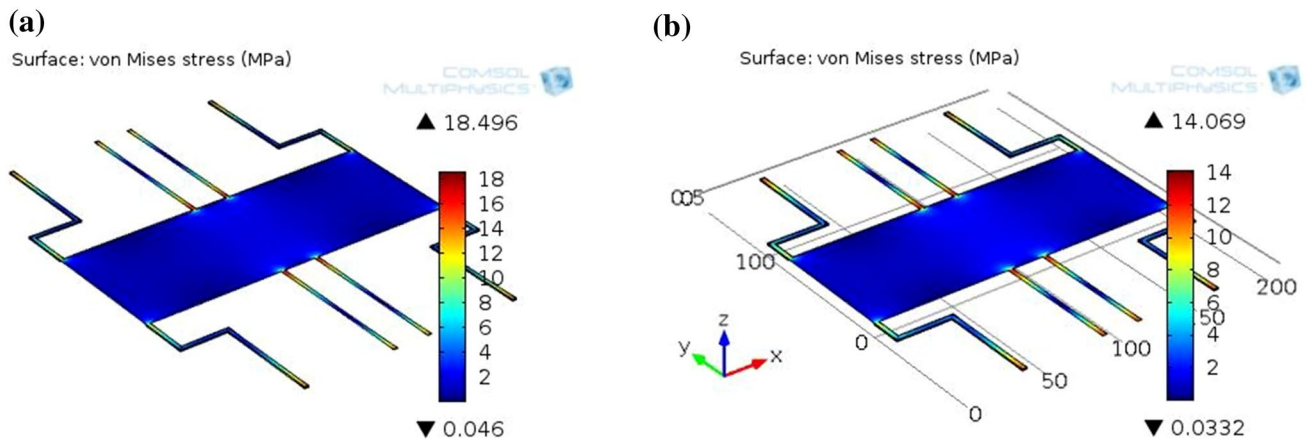


Fig. 8 Von Mises stress simulations for the optimized models. **a** Model a and Model c and **b** Model b

Table 9 Materials' properties

Material	Density (g/cm ³)	Young's modulus (GPa)	Poisson ratio	Dielectric constant
Si	2.3	170	0.26	–
SiO _x	2.2	73	0.17	4.99
Al	2.7	70	0.36	–

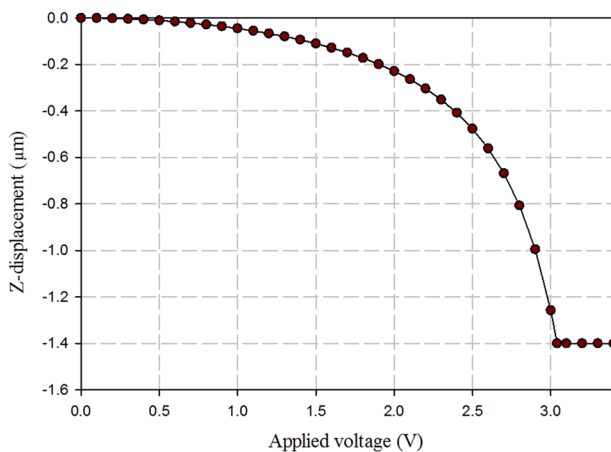


Fig. 9 Applied voltages vs. membrane's vertical displacement

illustrate that the geometric parameters' settings for achieving both low spring constant and small von Mises stress simultaneously do not coincide. Generally, Taguchi method is better to be used for optimizing a single response or one design objective with many controllable parameters or factors, as in (Fahsyar and Soin 2012; Su and Yeh 2011). For this multi-response optimization, if all the responses have same parameters' setting, then the optimized result is obtained; if the responses

have conflict parameters' setting, then a trade-off technique among them is needed. Here, in order to obtain the trade-off parameters for low spring constant and small von Mises stress designs, a further calculation of multi-response optimization, namely WPCA was conducted, as mentioned in Fig. 3.

3.2 Weighted principal component analysis

Principal component analysis (PCA) is a multivariate statistical method used for data reduction purpose. The basic idea is to represent a set of variables by a smaller number of variables known as principal components. It involves a mathematical procedure that reduces the dimensions of a set of variables by reconstructing them into uncorrelated combinations (Wu and Chyu 2004). However, there are still some obvious shortcomings in the PCA method. First, only the principal components with eigenvalues ≥ 1 are chosen to be analysed in PCA. Second, when more than one principal component (eigenvalue ≥ 1) is selected, the required trade-off for a feasible solution is unknown; and third, the multi-response performance index cannot replace the multi-response solution when the chosen principal component can only be explained by total variation (Liao 2006). WPCA is a method bases on PCA while all principal components and their weights are taken into consideration. In order to completely explain variation for all responses, WPCA uses the explained variation as the weight to combine all principal components into a multi-response performance index (MPI) for the further optimization results produced (Liao 2006). Experimental results using WPCA have been reported by some researchers to provide higher accuracy than the conventional PCA (Fan et al. 2011; Pinto da Costa et al. 2011).

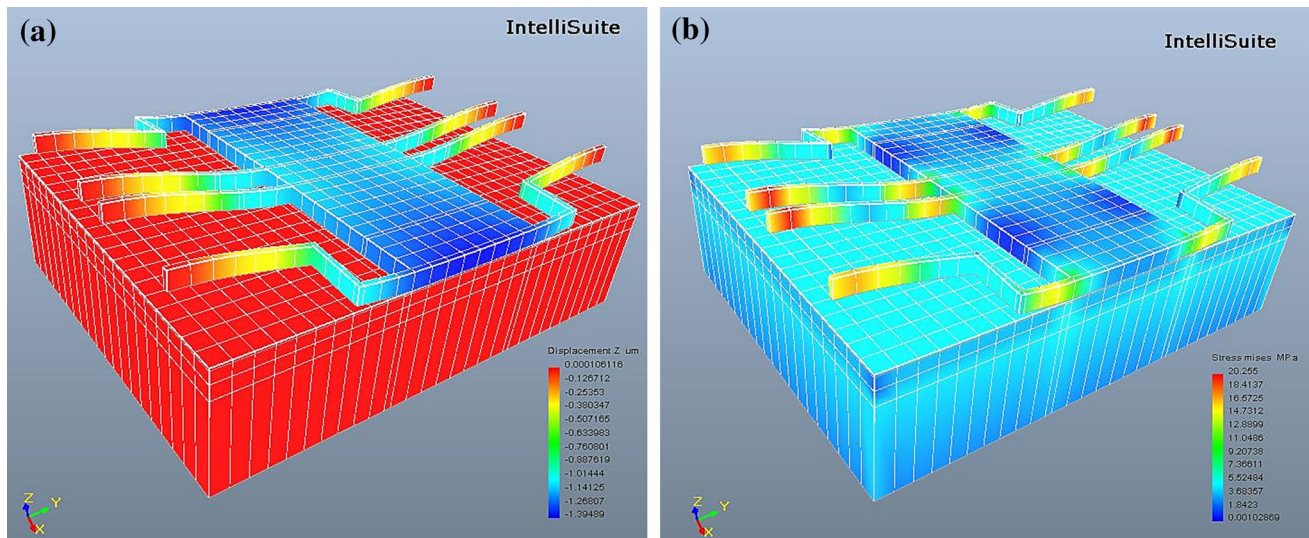


Fig. 10 3D view of the optimized RF-MEMS switch's simulations with $V_p = 3.04$ V. **a** Z-displacement distribution and **b** Von Mises stress distribution

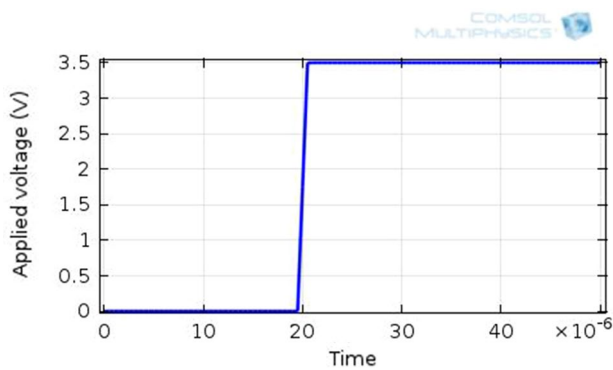


Fig. 11 Voltage load in time domain

3.2.1 WPCA procedure

In order to compute WPCA and obtain the MPI, a simple procedure needs to be carried out as follows. First, using (4) (Jaafar et al. 2009) normalizes the S/N values for all the responses. The normalized value can get rid of the difference between different units and it should be located in the range of 0 to 1. Second, PCA is performed by using the normalized S/N values to obtain the values of explained variation of all the responses, the eigenvalues and eigenvectors of each principal component. Last step is to calculate MPI by (5), where all the principal components and their explained variations or weights are considered (Liao 2006).

$$x_i^*(j) = \frac{x_i(j) - x_i(j)^-}{x_i(j)^+ - x_i(j)^-} \tag{4}$$

where, $x_i(j)$ means the S/N value of j th response at i th experiment number, $x_i^*(j)$ is the normalized response, $x_i(j)^+$

is the maximum value of $x_i(j)$ at j th response, and $x_i(j)^-$ is the minimum value of $x_i(j)$ at j th response.

$$MPI = \sum_{j=1}^r W_j Z_j \tag{5}$$

where, Z_j is the j th principal component which can be obtained by (6); W_j is the weight (or explained variation) of j th principal component; and r refers to the total of response number.

$$Z_j = \sum_{i=1}^p a_{ji} x_i^*(j) \tag{6}$$

where, a_{ji} is the eigenvector which satisfies the relation of $\sum_{i=1}^p a_{ji}^2 = 1$.

3.2.2 Multi-response optimization by WPCA

Following the WPCA procedures introduced in last part, the S/N normalized values for both spring constant and maximum von Mises stress were calculated by (4), as shown in Table 5. Add-Ins tool of XLSTAT in Microsoft Excel® has been used to compute PCA, where the normalized S/N values of k and $\sigma_{v(max)}$ were set as the Observations or variables; and the simulation run numbers were set as the Observation labels. After the calculation, a complete PCA datasheet was displayed in Microsoft Excel®. Table 6 summarized some important PCA data.

By using (5), MPI can be calculated as below (7) and the values were displayed in the form of the standard OA of L_9 , as shown in Table 5. Calculation of the mean values

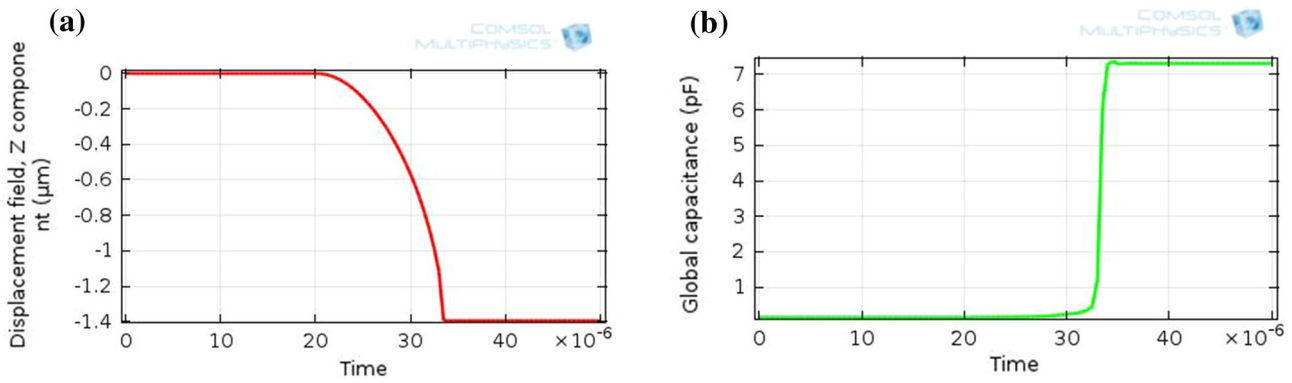


Fig. 12 Simulation of the optimized RF-MEMS switch in time domain. **a** Membrane’s movement, and **b** capacitances of switch-on and switch-off

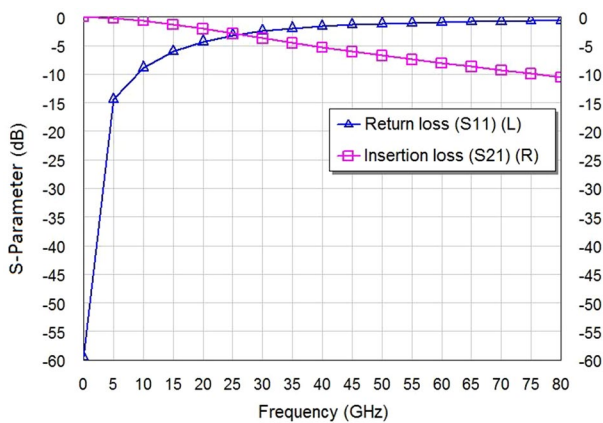


Fig. 13 S-parameters of switch-on state

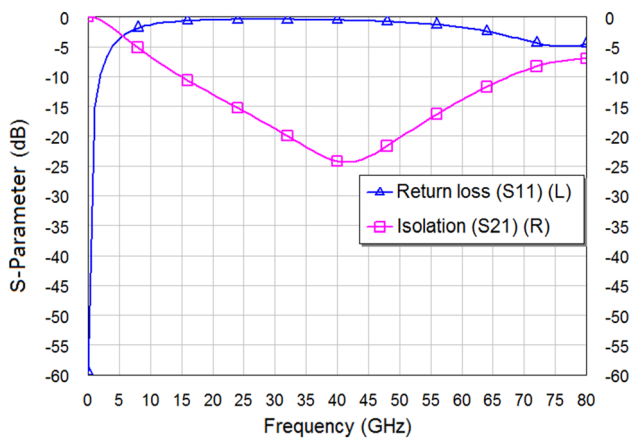


Fig. 14 S-parameters of switch-off state

of MPI at each level for each factor allows us to obtain the final optimized combinations for the multiple responses. Specific to this case, the values are $w_2(L1)_3(L2)_1(L3)_2$, as displayed in Table 7 and Fig. 6, where $w = w_2 = 2.5 \mu\text{m}$,

$L1 = (L1)_3 = 30 \mu\text{m}$, $L2 = (L2)_1 = 30 \mu\text{m}$, and $L3 = (L3)_2 = 65 \mu\text{m}$.

$$\begin{aligned}
 MPI &= W_1 Z_1 + W_2 Z_2 \\
 &= 0.61913 \times [Z1_{(k)} \times x_i^*(1) + Z1_{(\sigma_{v(max)})} \times x_i^*(2)] \\
 &\quad + 0.38087 \times [Z2_{(k)} \times x_i^*(1) + Z2_{(\sigma_{v(max)})} \times x_i^*(2)]
 \end{aligned}
 \tag{7}$$

3.3 Summary of the optimized results

The RF-MEMS switch’s beams geometric optimization with the objectives of (1) low spring constant, (2) small maximum von Mises stress, (3) multiple responses has been done separately in the aforementioned sections. The geometric parameters were set differently according to the different objectives, as shown the summary in Table 8. The same optimized result for multi-response design (Model c) and low spring constant design (Model a) is mainly due to the selection of the parameters’ value range (in Table 2). This reasonable values range was estimated and selected by the limitations of whole chip design dimension, fabrication, as well as the design specifications. A trade-off Model c is supposed to be different from both Model a and Model b; Model b stands for the optimum condition for small von Mises stress ($\sigma_{v(max)}$) design. But after the calculation, Model c is more inclined to Model a, this is because: (1) the beam lengths of L1, L2 and L3 have much less effect on the $\sigma_{v(max)}$ (Fig. 5b, totally around 5 %) comparing k (Fig. 5a, totally around 68 %); (2) the optimized beam width for both $\sigma_{v(max)}$ ($w = 3 \mu\text{m}$) and k ($w = 2.5 \mu\text{m}$) are very close. Moreover, both Model a and Model b’s contribution has been considered and calculated by (7). After validation, Model c has spring constant of $V_p = 3.04 \text{ V}$ and maximum von Mises stress of $\sigma_{v(max)} = 20.255 \text{ MPa}$, as shown in Figs. 7 and 8, which meets with our design objective, further different

parameters' value range has not been tried (as shown the work flow in Fig. 3). However, WPCA is a necessary step when there is different optimized parameters' setting for different responses.

4 Simulations of the optimized RF-MEMS switch

The optimized geometric dimensions have been obtained by Taguchi method and WPCA. In this part, its static property, dynamic property, and RF performance is investigated by FEM simulations.

4.1 Electro-mechanical analysis

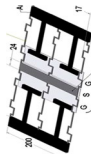
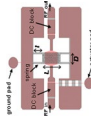
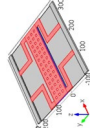
The simulation model is established in accordance with the dimensions in Table 1 and the multi-response optimized values in part 3. The materials' properties of each layer can be found in Table 9, which directly follows the setting from the IntelliSuite v8.7[®] software's material library, except the thin silicon dioxide layer's dielectric constant of 4.99. The boundary conditions are set as: (1) the bottom plate of silicon (Si) substrate is fixed; (2) all the beams' ends are set as fixed face; and (3) potential of the signal line is set to zero to simplify the simulation; and the membrane is assigned with varying voltage load, in order to find V_p . The model is then meshed using rectangular elements of less than 10 μm .

The simulation result of membrane's vertical displacement with the varying applied voltage is displayed in Fig. 9. It can be seen that the membrane totally collapses on the bottom plate at the voltage of 3.04 V which is the optimized switch's V_p . Figure 10 shows 3D results of the membrane's vertical displacement and stress distribution during actuated state, respectively, where the obtained $\sigma_{v(max)}$ of 20.255 MPa is much less than the yield strength of Al, 90 MPa (Dai et al. 2005).

4.2 Actuation time and capacitance

The RF-MEMS switch's actuation time is limited by the mechanical structure and basically is inversely proportional to the membrane and beam's total resonant frequency (Mafinejad et al. 2013). A time dependent simulation by Comsol Multiphysics 4.3[®] has been conducted to estimate this optimized RF-MEMS switch's actuation time. The boundary conditions are set similar as the previous simulation, except a step-up voltage load is applied on the membrane, as shown in Fig. 11. The high level voltage of the step function of 3.5 V is a bit higher than the V_p ; and its rising time is adjusted within 1 μs . Then the simulated results of membrane's movement and switch's capacitances are presented in Fig. 12. Figure 12a shows that, when applied voltage at low stage (near to 0 V), the membrane almost

Table 10 Comparison of developed capacitive RF-MEMS switches

Electrostatic capacitive RF-MEMS Switch	Dai et al. (2006)	Fouladi et al. (2010)	Badia et al. (2012)	Persano et al. (2012)	Ya et al. (2013)	This work
Structure						
Actuation Voltage	7 V	82 V	23.6 V	25 V	3 V	3.04 V
Spring Constant	0.27 N/m	-	1.43 N/m	-	0.65 N/m	1.3 N/m
Air Gap	3.5 μm	-	3 μm	3 μm	2.2 μm	1.397 μm
Dielectric	1.1 μm SiO ₂ $\epsilon_r = 3.9$	0.73 μm SiO ₂ $\epsilon_r = 3.9$	300 nm AlN $\epsilon_r = 9.8$	300 nm Si ₃ N ₄ $\epsilon_r = 6-7$	0.1 μm SiO ₂ $\epsilon_r = 4.99$	0.1 μm SiO ₂ $\epsilon_r = 4.99$
Insertion Loss	-3.1 dB @40 GHz	-0.98 dB @20 GHz	-0.68 dB @40 GHz	<0.8 dB @ K-band	-	-5.65 dB @40 GHz
Isolation	-15 dB @40 GHz	-17.9 dB @20 GHz	-35.75 dB @40 GHz	>30 dB @ K-band	-	-24.38 dB @40 GHz
Capacitance Ratio Cr (= C_d/C_u)	-	91 (2.1pF/23fF)	9.87 (1.266pF/128.32fF)	16.3 (2.2pF/0.135pF)	100 (10.36pF/0.1pF)	52 (7.31pF/0.14pF)
Actuation Time	8.2 μs	49 μs	-	-	-	13.5 μs
Fabrication Process	TSMC0.35 μm CMOS + post-process	TSMC0.35 μm CMOS + post-process	Seven-mask process (not CMOS)	Eight-mask process (not CMOS)	MIMOS0.35 μm CMOS + post-process (one mask)	MIMOS0.35 μm CMOS + post-process (maskless)

keeps at its original position (z -displacement = 0 μm). Once the applied voltage is increased to 3.5 V at $t = 20 \mu\text{s}$; the beams start to bend down until the membrane reaches the maximum displacement at $t = 33.5 \mu\text{s}$. Therefore, the actuation time of the optimized switch is 13.5 μs . Figure 12b illustrates the switch-on and switch-off capacitances are 0.14 and 7.31 pF, respectively. The capacitance ratio of the optimized switch is around 52.

4.3 RF performance

Electromagnetic (EM) simulator of AWR Design Environment 10[®] has been used to compute the RF responses (S-parameters) of the RF-MEMS switch. When the switch state is ON, no actuation occurs and the RF signal passes underneath the membrane with relatively little attenuation. Its return loss (S11) and insertion loss (S21) is presented in Fig. 13, where return loss is -1.51 dB and insertion loss is -5.65 dB at 42 GHz. This relatively high insertion loss is mainly due to the small fixed gap (g_0) between two metal layers and low-resistivity silicon substrate which is limited by the CMOS fabrication process. When the switch is actuated, the metal-dielectric-metal sandwich produces a low impedance path to the surrounding CPW grounds (Yao et al. 1999); this prevents the RF signal from traversing beyond the switch, and the switch state is OFF. During this state, the return loss (S11) of -0.60 dB and isolation (S21) of -24.38 dB at the frequency of 40 GHz is shown in Fig. 14.

Table 10 presents the comparison of our work with some typical developed capacitive RF-MEMS switches. It shows our proposed switch's V_p is low enough to be integrated with most CMOS circuitry while other properties are kept in a reasonable range.

5 Conclusion

A novel shunt capacitive RF-MEMS switch using standard 0.35 μm CMOS process has been designed, optimized and simulated. The RF-MEMS switch employs four supporting folded beams and four straight beams as DC voltage supply paths. Both Taguchi method and WPCA have been used to optimize the switch's geometric parameters. A complete optimization methodology for multiple responses has been developed in this work. By employing a L_9 orthogonal array and calculation of the S/N from each simulation results, the best combination of the four parameters for the nominated spring constant design is $w_2(L1)_3(L2)_1(L3)_2$; and the best combination for smallest von Mises stress design is $w_3(L1)_1(L2)_2(L3)_1$. By using WPCA and calculating the MPI as well as their mean values at each level for each parameter, the multi-response optimized

design is $w_2(L1)_3(L2)_1(L3)_2$, where, $w = w_2 = 2.5 \mu\text{m}$, $L1 = (L1)_3 = 30 \mu\text{m}$, $L2 = (L2)_1 = 30 \mu\text{m}$ and $L3 = (L3)_2 = 65 \mu\text{m}$.

For the multi-response optimized RF-MEMS switch, a very low pull-in voltage of 3.04 V can be achieved and compatible with the most CMOS power supply requirements. The simulated actuation time of the optimized switch is 13.5 μs and the capacitance ratio is 52. The insertion loss and isolation is -5.65 dB and -24.38 dB at the frequency of 40 GHz, respectively. The whole optimization methodology not only can be applied for RF-MEMS switch's geometric parameters' optimization, but also can be used for other RF-MEMS devices' optimization process, especially with multiple responses or objectives.

Acknowledgments The research is collaborative effort between University of Malaya and International Islamic University Malaysia. All authors would like to thank the financial support by the RACE fund (RACE 12-006-0006), UM CR 004-2013, and University Malaya High Impact Research Grant (UM.C/HIR/MOHE/ENG/19).

References

- Afrang S, Abbaspour-Sani E (2006) A low voltage MEMS structure for RF capacitive switches. *Prog Electromagn Res* 65:157–167. doi:10.2528/PIER06093001
- Badia M-B, Buitrago E, Ionescu AM (2012) RF MEMS shunt capacitive switches using AlN compared to dielectric. *J Microelectromech Syst* 21(5):1229–1240. doi:10.1109/JMEMS.2012.2203101
- Balaraman D, Bhattacharya SK, Ayazi F, Papapolymerou J (2002) Low-cost low actuation voltage copper RF MEMS switches. In: *IEEE MTT-S International Microwave Symposium Digest 2002*, vol 2, pp 1225–1228. doi:10.1109/MWSYM.2002.1011879
- Bao MH (2000) *Micro mechanical transducers: pressure sensors, accelerometers and gyroscopes*, vol 8. Elsevier
- Chan R, Lesnick R, Becher D, Feng M (2003) Low-actuation voltage RF MEMS shunt switch with cold switching lifetime of seven billion cycles. *J Microelectromech Syst* 12(5):713–719. doi:10.1109/JMEMS.2003.817889
- Chen M-T, Harichandran R (1998) Statistics of the von Mises stress response for structures subjected to random excitations. *Shock Vib* 5(1):13–21. doi:10.1155/1998/162424
- Cho I-J, Yoon E (2010) Design and fabrication of a single membrane push-pull SPDT RF MEMS switch operated by electromagnetic actuation and electrostatic hold. *J Micromech Microeng* 20(3):035028. doi:10.1088/0960-1317/20/3/035028
- Chu C-H, Shih W-P, Chung S-Y, Tsai H-C, Shing T-K, Chang P-Z (2007) A low actuation voltage electrostatic actuator for RF MEMS switch applications. *J Micromech Microeng* 17(8):1649. doi:10.1088/0960-1317/17/8/031
- Dai C-L, Chen J-H (2006) Low voltage actuated RF micromechanical switches fabricated using CMOS-MEMS technique. *Microsyst Technol* 12(12):1143–1151. doi:10.1007/s00542-006-0243-7
- Dai C, Peng H, Liu M, Wu C, Yang L (2005) Design and fabrication of RF MEMS switch by the CMOS process. *Tamkang J Sci Eng* 8(3):197. doi:10.6180/jase.2005.8.3.03
- Daneshmand M, Fouladi S, Mansour RR, Lisi M, Stajcer T (2009) Thermally actuated latching RF MEMS switch and its characteristics. *IEEE Trans Microw Theory Tech* 57(12):3229–3238. doi:10.1109/TMTT.2009.2033866

- Fahsyar PNA, Soin N (2012) Optimization of design parameters for radiofrequency identification tag rectifier using taguchi methods. *IETE Tech Rev* 29(2):157–161. doi:10.4103/0256-4602.95387#.VVIsk_yUfNc
- Fan Z, Liu E, Xu B (2011) Weighted principal component analysis. In *Artificial Intelligence and Computational Intelligence*, Springer, pp 569–574. doi:10.1007/978-3-642-23896-3_70
- Fouladi S, Mansour RR (2010) Capacitive RF MEMS switches fabricated in standard 0.35-CMOS technology. *Microw Theory Tech IEEE Trans* 58(2):478–486. doi:10.1109/TMTT.2009.2038446
- Fraley S, Oom M, Terrien B, Date J (2006) Design of experiments via Taguchi methods: orthogonal arrays. *The Michigan chemical process dynamic and controls open text book, USA, vol 2. No.3. p 4.* https://controls.engin.umich.edu/wiki/index.php/Design_of_experiments_via_taguchi_methods:_orthogonal_arrays
- Glickman M, Tseng P, Harrison J, Niblock T, Goldberg IB, Judy JW (2011) High-performance lateral-actuating magnetic MEMS switch. *J Microelectromech Syst* 20(4):842–851. doi:10.1109/JMEMS.2011.2159096
- Gong Y, Zhao F, Xin H, Lin J, Bai Q. Simulation and Optimal Design for RF MEMS Cantilevered Beam Switch. In: *IEEE International Conference on Future Computer and Communication 2009 (FCC'09)*, pp 84–87. doi:10.1109/FCC.2009.45
- Gupta RK (1997) Electrostatic pull-in test structure design for in situ mechanical property measurements of microelectromechanical systems (MEMS). Doctoral dissertation, Massachusetts Institute of Technology. doi=10.1.1.142.1713&rep=rep1&type=pdf. <http://citeseerx.ist.psu.edu/viewdoc/download;jsessionid=F890E3D4544E36D79977815A8EC7E36E?>
- Jaafar H, Sidek O, Miskam A, Korakkottil S (2009) Design and simulation of microelectromechanical system capacitive shunt switches. *Am J Eng Appl Sci* 2(4):655. doi:10.3844/ajeassp.2009.655.660
- Kim J-M, Lee S, Park J-H, Baek C-W, Kwon Y, Kim Y-K (2010) Electrostatically driven low-voltage micromechanical RF switches using robust single-crystal silicon actuators. *J Micromech Microeng* 20(9):095007. doi:10.1088/0960-1317/20/9/095007
- Kuwabara K, Sato N, Shimamura T, Morimura H, Kodate J, Sakata T, et al. (2006) RF CMOS-MEMS switch with low-voltage operation for single-chip RF LSIs. In: *IEEE International Electron Devices Meeting 2006 (IEDM'06)*, pp 1–4. doi:10.1109/IEDM.2006.346891
- Lakamraju NV, Phillips SM (2005) Bi-stable RF MEMS switch with low actuation voltage. *Proc Int Symp Microelectron.* http://engr.case.edu/liberatore_vincenzo/NetBots/NewimapsPhillips2.pdf
- Lee S-D, Jun B-C, Kim S-D, Park H-C, Rhee J-K, Mizuno K (2006) An RF-MEMS switch with low-actuation voltage and high reliability. *J Microelectromech Syst* 15(6):1605–1611. doi:10.1109/JMEMS.2006.886394
- Li T-S, Su C-T, Chiang T-L (2003) Applying robust multi-response quality engineering for parameter selection using a novel neural-genetic algorithm. *Comput Ind* 50(1):113–122. doi:10.1016/S0166-3615(02)00140-9
- Liao H-C (2006) Multi-response optimization using weighted principal component. *Int J Adv Manuf Technol* 27(7–8):720–725. doi:10.1007/s00170-004-2248-7
- Mafinejad Y, Kouzani A, Mafinezhad K, Mashad I (2013) Review of low actuation voltage RF MEMS electrostatic switches based on metallic and carbon alloys. *J Microelectron Electron Compon Mater* 43(2):85–96. <http://hdl.handle.net/10536/DRO/DU:30055302>
- Meng T, Butler C (1997) Solving multiple response optimisation problems using adaptive neural networks. *Int J Adv Manuf Technol* 13(9):666–675. doi:10.1007/BF01350825
- Park SH, Antony J (2008) *Robust design for quality engineering and Six Sigma*: World Scientific
- Park J-H, Lee H-C, Park Y-H, Kim Y-D, Ji C-H, Bu J et al (2006) A fully wafer-level packaged RF MEMS switch with low actuation voltage using a piezoelectric actuator. *J Micromech Microeng* 16(11):2281. doi:10.1088/0960-1317/16/11/005
- Peroulis D, Pacheco SP, Sarabandi K, Katehi LP (2003) Electromechanical considerations in developing low-voltage RF MEMS switches. *IEEE Trans Microw Theory Tech* 51(1):259–270. doi:10.1109/TMTT.2002.806514
- Persano A, Tazzoli A, Farinelli P, Meneghesso G, Siciliano P, Quaranta F (2012) K-band capacitive MEMS switches on GaAs substrate: design, fabrication, and reliability. *Microelectron Reliab* 52(9):2245–2249. doi:10.1016/j.microrel.2012.06.008
- Philippine MA, Sigmund O, Rebeiz GM, Kenny TW (2013) Topology optimization of stressed capacitive RF MEMS switches. *J Microelectromech Syst* 22(1):206–215. doi:10.1109/JMEMS.2012.2224640
- Pinto da Costa JF, Alonso H, Roque L (2011) A weighted principal component analysis and its application to gene expression data. *IEEE/ACM Trans Comput Biol Bioinform (TCBB)* 8(1):246–252. doi:10.1109/TCBB.2009.61
- Rebeiz GM (2003) *RF MEMS—theory, design, and technology*. John Wiley & Sons Inc, Hoboken, p 32
- Roy RK (2010) *A primer on the Taguchi method*: Society of Manufacturing Engineers
- Shalaby MM, Wang Z, Chow LL-W, Jensen BD, Volakis JL, Kurabayashi K et al (2009) Robust design of RF-MEMS cantilever switches using contact physics modeling. *IEEE Trans Industr Electron* 56(4):1012–1021. doi:10.1109/TIE.2008.2006832
- Su C-T, Yeh C-J (2011) Optimization of the Cu wire bonding process for IC assembly using Taguchi methods. *Microelectron Reliab* 51(1):53–59. doi:10.1016/j.microrel.2010.09.007
- Taguchi G, Clausing D, Watanabe LT (1987) *System of experimental design: engineering methods to optimize quality and minimize costs (vol 2)*: UNIPUB/Kraus International Publications White Plains, New York
- Wu F-C, Chyu C-C (2004) Optimization of correlated multiple quality characteristics robust design using principal component analysis. *J Manuf Syst* 23(2):134–143. doi:10.1016/S0278-6125(05)00005-1
- Wey IC, Huang CH, Chow HC (2002) A new low-voltage CMOS 1-bit full adder for high performance applications. In: *Proceedings of IEEE Asia-Pacific Conference on ASIC, 2002*, pp 21–24. doi:10.1109/APASIC.2002.1031522
- Ya ML, Nordin AN, Soin N, Design and analysis of a low-voltage electrostatic actuated RF CMOS-MEMS switch. In: *IEEE Regional Symposium on Micro and Nanoelectronics (RSM2013)*. pp 41–44. doi:10.1109/RSM.2013.6706468
- Yao ZJ, Chen S, Eshelman S, Denniston D, Goldsmith C (1999) Micromachined low-loss microwave switches. *Microelectromech Syst J* 8(2):129–134. doi:10.1109/84.767108
- Yusoff Y, Zoofakhar AS, Aman S, Ahmad MR (2004) Design and characterization of input and output (I/O) pads. In: *IEEE International Conference on Semiconductor Electronics (ICSE 2004)*, p 7. doi:10.1109/SMELEC.2004.1620941